Magnetic boson peak in classical spin glasses

Maiko Kofu [1,*] Seiko Ohira-Kawamura,[1] Naoki Murai,[1] Rieko Ishii [2] Daigorou Hirai [2,3]
Hiroshi Arima [4] and Kenichi Funakoshi[4]

[1]*J-PARC Center, Japan Atomic Energy Agency, Tokai, Ibaraki 319-1195, Japan*
[2]*Institute for Solid State Physics, University of Tokyo, Kashiwa, Chiba 277-8581, Japan*
[3]*Department of Applied Physics, Nagoya University, Nagoya 464-8603, Japan*
[4]*Comprehensive Research Organization for Science and Society, Tokai, Ibaraki 319-1106, Japan*

We revisited spin dynamics in archetypical classical spin-glass (SG) systems, such as $Cu_{1-x}Mn_x$ ($x = 0.017$, 0.034, and 0.067) dilute alloys and iron aluminosilicate glass, using a modern neutron scattering spectrometer with high neutron flux. The former is crystalline, and the latter is amorphous, where their SG state is well separated from magnetically ordered phases. Bose-scaled localized magnetic excitations were observed in both compounds below the spin-freezing temperature (T_f). The spectrum exhibits a maximum at low energy and a broad tail on the high-energy side. The excitation energy tends to be higher for the material with higher T_f. Above T_f, the spectrum considerably changes with temperature, thereby indicating the emergence of the magnetic relaxation process. The magnetic excitation in the SG state has much in common with the boson peak in structural glasses. We consider that the Bose-scaled broad excitation peak is an elementary excitation inherent in disordered systems.

DOI: 10.1103/PhysRevResearch.6.013006

I. INTRODUCTION

Spin glasses (SGs) are ubiquitous in magnetic materials with competing interactions and randomness. Time, temperature, and magnetic-field-dependent magnetic relaxation describe the characteristics of SGs and have been studied experimentally and theoretically [1–4]. However, excitation features in an SG state remain elusive. In the early stages of SG research, attempts have been made to probe spin excitations of the SG state by neutron spectroscopy; however, no noticeable observations have been reported [5]. Furthermore, most theoretical calculations have failed to derive spin waves in the SG regime. Only a few computer simulations of Heisenberg SGs (e.g., $Cu_{1-x}Mn_x$ dilute alloy) have suggested the existence of localized modes [6].

Recently, we investigated magnetic excitations in a magnetic ionic liquid (C4mimFeCl$_4$: 1-butyl-3-methylimidazolium tetrachloroferrate) by inelastic neutron scattering (INS). C4mimFeCl$_4$ exhibits an SG transition with a spin-freezing temperature (T_f) of 0.4 K in the glassy state and antiferromagnetic ordering in the crystalline state [7]. In the SG state, localized magnetic excitations were found unlike the spin-wave excitations in the ordered phase of the crystalline sample. The localized excitation is scaled by the Bose factor below T_f while gradually disappearing above T_f. The magnetic excitation in the SG state is highly reminiscent of the *boson peak*, originating from low-frequency vibrational modes, commonly observed in structural glasses [8], and can be termed a *magnetic boson peak* (MBP).

In this paper, we report on INS investigations of two classical Heisenberg SGs, $Cu_{1-x}Mn_x$ dilute alloys and iron aluminosilicate glass (FeO–Al$_2$O$_3$–SiO$_2$: FeAlSiO). The former is crystalline, and the latter is amorphous, where their SG states are well separated from magnetically ordered phases. We show that the MBP is usually observed in these compounds. The SG-like behavior has been reported in various magnetic materials, including dilute magnetic alloys, mixed-phase magnetic oxides, intermetallics, high-T_c superconductors, and frustrated magnets, However, SG frequently appears near the ordered phase, and magnetic excitations originating from the ordered phase might be observed in many systems. Therefore, herein, we focus on the two compounds to experimentally search for excitations intrinsic to the SG state.

II. MATERIALS AND METHODS

A. Sample preparation

The $Cu_{1-x}Mn_x$ alloys with nominal compositions of $x = 0.0165$, 0.0335, and 0.0669 were prepared from pure Cu (99.9995%, Sigma-Aldrich) and Mn (99.9%, Nilaco) The Cu and Mn were arc-melted several times in an argon atmosphere. The alloys were vacuum sealed and annealed at 750 °C for 300 h. The actual compositions were estimated by inductively coupled plasma (ICP) analysis.

The $(FeO)_{0.452}(Al_2O_3)_{0.088}(SiO_2)_{0.46}$ glass was prepared by rapid quenching like in Refs. [9,10]. The mixture of Fe$_2$O$_3$ (99.9%, Kojundo Chemical Lab), Al$_2$O$_3$ (99.99%, Kojundo Chemical Lab), and SiO$_2$ (99.9%, Kojundo Chemical Lab) powders was melted at 1400 °C for ~60 min in a graphite crucible and quenched in argon. The Fe, Al, and Si composi-

*maiko.kofu@j-parc.jp

TABLE I. Compositions, freezing temperatures (T_f's), Curie-Weiss temperatures (θ), and effective paramagnetic moments (μ_{eff}) for $Cu_{1-x}Mn_x$ and $FeO–Al_2O_3–SiO_2$ studied in this paper. The parameters of C4mimFeCl$_4$ [7] are also shown for comparison.

x^a	x^b	T_f (K)	θ (K)	μ_{eff} (μ_B)
$Cu_{1-x}Mn_x$				
0.0165	0.0176	12.4	10.1	4.58
0.0335	0.0337	20.2	27.1	5.16
0.0669	0.0658	32.0	56.0	5.10
FeO-Al$_2$O$_3$-SiO$_2$ (FeAlSiO)				
41.5:16.2:42.3	41.4:16.0:42.6	9.8	−88.9	5.26
C4mimFeCl$_4$				
		0.4	−4.08	5.56

^{a}Nominal composition.
^{b}Estimated from ICP or SEM.

tion was estimated by scanning electron microscopy (SEM), and the homogeneity of the sample was confirmed.

The estimated compositions of $Cu_{1-x}Mn_x$ alloys and FeAl-SiO glass are listed in Table I, which correlate well with the nominal values. The samples used for ICP or SEM, magnetic susceptibility, and neutron scattering were cut from the same ingots.

B. Magnetic susceptibility

Direct current (DC) magnetic susceptibilities were measured using a superconducting quantum interference device (SQUID) magnetometer (MPMS3, Quantum Design Co.). Figure 1 displays the zero-field-cooled (ZFC) and field-cooled (FC) susceptibilities measured on heating under a DC field of 10 Oe. The T_f's are defined as the temperatures at which irreversibility between the ZFC and FC susceptibilities emerges. The ZFC curve exhibits a sharp maximum at $T \approx T_f$. To estimate Curie-Weiss temperatures (θ) and effective paramagnetic moments (μ_{eff}), the magnetic susceptibility was measured under 1000 Oe at 2–350 K. The susceptibility in the paramagnetic region well above T_f ($T > 4T_f$) was fitted with the Curie-Weiss law $\chi = N\mu_{eff}^2/3k_B(T - \theta)$. The obtained parameters are summarized in Table I and consistent with literature data for $Cu_{1-x}Mn_x$ alloys [11] and FeAlSiO
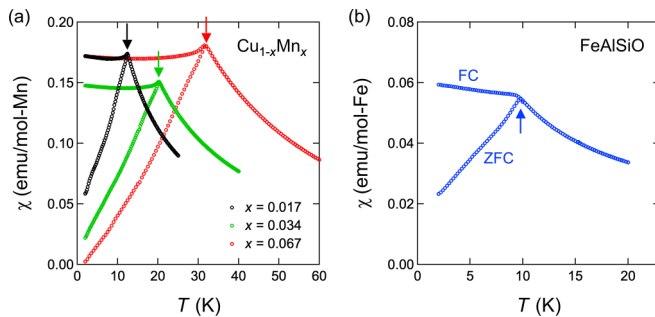

FIG. 1. Temperature dependence of magnetic susceptibility of (a) $Cu_{1-x}Mn_x$ polycrystals and (b) FeAlSiO glass. The arrows indicate the freezing temperatures (T_fs). The data were obtained in a DC field of 10 Oe.

glass [12,13]. Note that the positive value of θ suggests that ferromagnetic interaction is dominant in $Cu_{1-x}Mn_x$.

C. Neutron scattering

Neutron scattering measurements were performed using a disk-chopper spectrometer AMATERAS [14] at the Materials and Life Science Experimental Facility (MLF), J-PARC. Approximately 10 g of $Cu_{1-x}Mn_x$ alloys and 2 g of FeAlSiO glass were used in the experiment. The samples were fixed to thin aluminum plates with aluminum wire and mounted to closed-cycle refrigerators. The frequency and phase of choppers were configured to select two E_i sets: $E_i = 18.7$ (0.82), 9.0 (0.27), 5.3 (0.12) meV, and 15.2 (0.60), 7.7 (0.21) meV. The parentheses denote the corresponding energy resolutions (full width at half maximum at the elastic position). The neutron scattering data were recorded at 3 K ($Cu_{0.983}Mn_{0.017}$), 3–200 K ($Cu_{0.966}Mn_{0.034}$ and FeAlSiO), and 3–60 K ($Cu_{0.933}Mn_{0.067}$). Pure Cu data with a similar mass were obtained at 3 K and used to estimate the instrumental background, elastic tail, and phonon contributions. The recorded data were analyzed using the software suite Utsusemi [15].

III. RESULTS

A. $Cu_{1-x}Mn_x$ alloy

Figure 2 shows color contour maps of INS intensities $I(Q, \omega)$ for $Cu_{1-x}Mn_x$ at $T = 3$ K. As with all $Cu_{1-x}Mn_x$ samples, a sharp signal was observed at ~4.2 meV, probably originating in multiple scattering events involving the sample and cryostat. The data of pure Cu at 3 K were subtracted to remove the background. The weak signal at ~4 meV in $x = 0.017$ is due to imperfect subtraction. Broad low-energy magnetic excitations were clearly observed in the low-Q region in all samples. The conelike scattering at $Q \sim 3$ Å^{-1} is due to phonon contributions. The energy scale of magnetic excitation increases as x increases. The scattering shows weak intensity modulation along Q, which is more pronounced for high-x samples. Moreover, the strong scattering appeared at $Q \approx 0$, which reflects the predominant ferromagnetic interaction.

Figure 3(a) shows the temperature evolution of the INS spectra for $Cu_{1-x}Mn_x$ with $x = 0.034$, obtained by integrating the data collected with $E_i = 9$ meV over $Q = [1.5, 2.1]$ Å^{-1}, where magnetic scattering is strong. The spectrum changes with temperature over the entire temperature range (3 K $\leqslant T \leqslant 200$ K). To determine whether the spectrum below T_f scales with the Bose factor, we obtained the imaginary part of the magnetic susceptibility as follows:

$$\chi''(Q, \omega) = \frac{\pi}{2}\mu_B^2\left(\frac{2}{\gamma r_0}\right)^2 \frac{1}{|F(Q)|^2\{1 + n(\omega)\}} \frac{k_i}{k_f} \frac{d^2\sigma}{d\Omega dE_f},$$

(1)

where $\gamma = -1.913$, $r_0 = 2.818 \times 10^{15}$ m; $F(Q)$ is the magnetic form factor for Mn^{2+}; $n(\omega) = \{\exp(\hbar\omega/k_BT) - 1\}^{-1}$ is the Bose population factor; and k_i and k_f are the incident and scattered neutron wave vectors, respectively. The Debye-Waller factor was not included because of the focus on
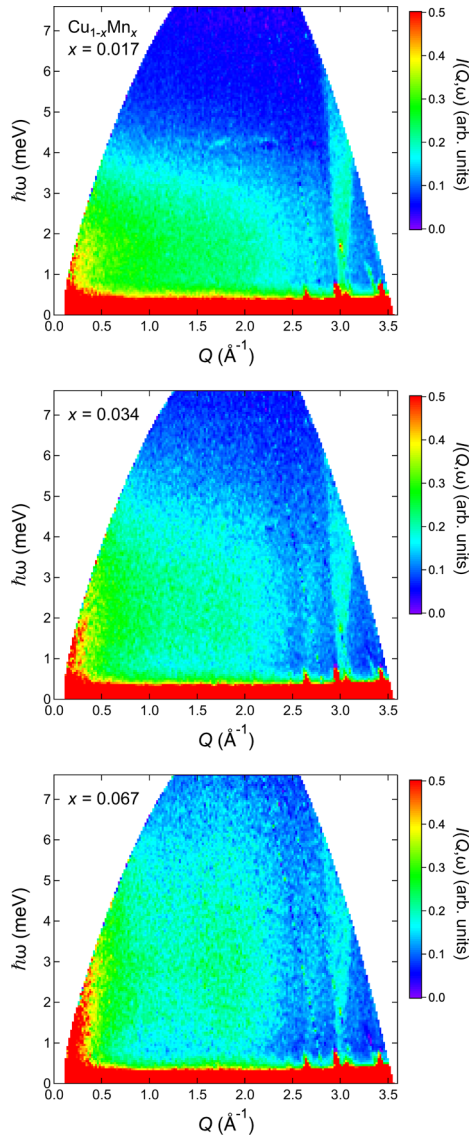
FIG. 2. Color contour maps of inelastic neutron scattering (INS) intensities for $Cu_{1-x}Mn_x$ at $T = 3$ K, collected with $E_i = 9$ meV. The data of pure Cu (background reference) were subtracted.

the low-Q region. The elastic tail and phonon contributions [16] were subtracted using the data of pure Cu. The $\chi''(Q, \omega)$ data were calibrated on an absolute scale by comparison with standard vanadium. The data collected with $E_i = 5.3$, 9.0, and 18.7 meV were employed to make the plots in the wide energy region. Figure 3(b) shows the obtained $\chi''(Q, \omega)$.

Below T_f, the excitation spectrum remains almost the same; it is scaled by the Bose factor. The spectrum exhibits a peak at ~ 2 meV, with a tail on the high-energy side. As shown in Fig. 3(c), the spectrum shape is almost independent of Q, suggesting localized excitation. The spectrum changes considerably when the temperature is raised above T_f, indicating that magnetic relaxation is activated. A similar temperature and Q dependence were observed in the $x = 0.067$ sample.

Fitting a Debye relaxation model,

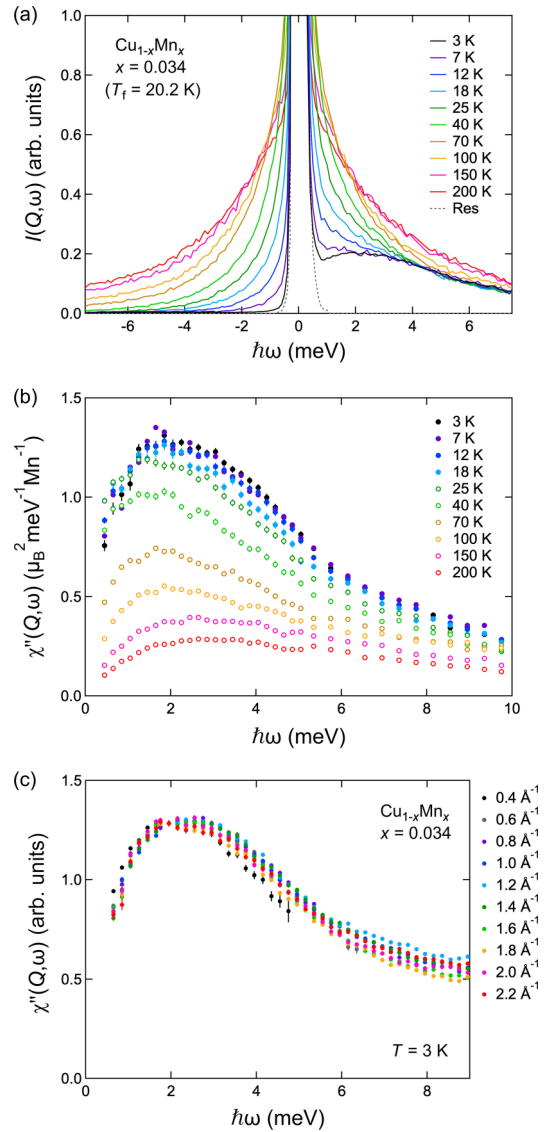$$\chi''(Q, \omega) = \chi'(Q) \frac{\Gamma \hbar \omega}{(\hbar \omega)^2 + \Gamma^2}, \qquad (2)$$

FIG. 3. (a) Temperature evolution of inelastic neutron scattering (INS) spectra collected with $E_i = 9.0$ meV at $Q = [1.5, 2.1]$ Å^{-1} for $Cu_{1-x}Mn_x$ with $x = 0.034$ ($T_f = 20.2$ K). Dashed curve represents a resolution function estimated from the data of pure Cu at 3 K. (b) Imaginary part of the magnetic susceptibility $\chi''(Q, \omega)$ at $Q = [1.5, 2.1]$ Å^{-1}. The data collected with $E_i = 5.3$, 9.0, and 18.7 meV are used. (c) Energy spectra at several Q positions at 3 K, where suitable scale factors are multiplied for comparison. The data collected with $E_i = 7.7$ and 15.2 meV are used. Error bars throughout this paper represent one standard deviation and are often smaller than symbol sizes.

to the energy spectrum was evaluated, as in the previous studies [17–23]. Here, $\chi'(Q)$ is the static susceptibility, and Γ is the relaxation rate, which roughly corresponds to the energy exhibiting a maximum in $\chi''(Q, \omega)$. The representative fit results are shown in Fig. 4(a). The Debye model can reproduce the spectrum at $T > 70$ K but not at $T < 40$ K. Temperature dependences of Γ and $\chi'(Q)$ are presented in Figs. 4(b) and 4(c), respectively. Here, Γ decreases with temperature, reflecting the slowing down of spin fluctuation. Above 70 K, Γ follows the Arrhenius law $\Gamma \propto \exp(-E_a/k_B T)$, where E_a
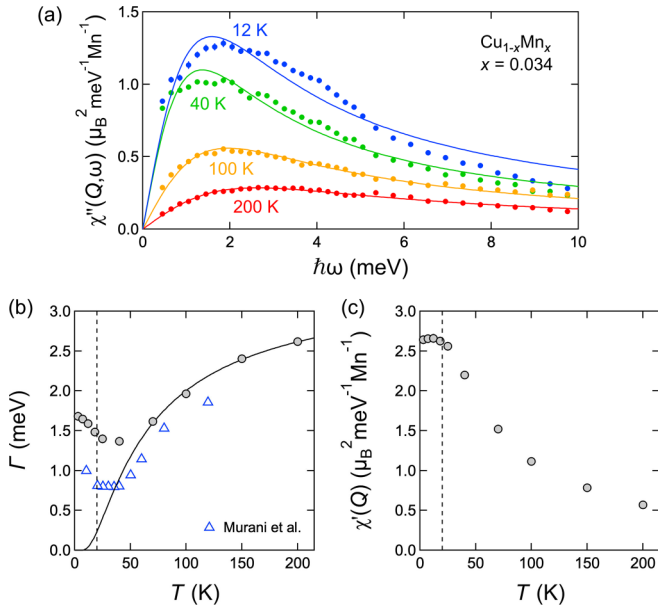
FIG. 4. (a) Fitting results with the Debye relaxation model to the spectra of $Cu_{1-x}Mn_x$ ($x = 0.034$) at $Q = [1.5, 2.1]$ Å^{-1}. See the text for details. (b) Relaxation rate Γ as a function of temperature. Solid curve represents the Arrhenius fit for data at $T > 70$ K, with the value of $E_a = 53(2)$ K. The literature data of $x = 0.03$ at $Q = 1$ Å^{-1} are shown as triangles [17]. (c) Static susceptibility $\chi'(Q)$ as a function of temperature. Vertical dashed lines in (b) and (c) denote T_f.

FIG. 5. Constant-$\hbar\omega$ cuts at (a) $\hbar\omega = [-0.15, 0.15]$ (elastic scattering) and (b) [1.6, 2.6] meV (excitation peak) for $x = 0.034$ and (c) $\hbar\omega = [-0.15, 0.15]$ and (d) [2, 3] meV for $x = 0.067$ at several temperatures. In (a) and (c), the data at high temperatures were subtracted to obtain magnetic elastic scattering, and the regions in the Bragg reflections from the $Cu_{1-x}Mn_x$ samples and Al holder were masked. In (b) and (d), the scale factors are multiplied for comparison. All the data shown were collected with $E_i = 9.0$ meV, with an energy resolution of 0.27 meV.

is the activation energy, shown as a solid curve. However, a significant deviation from the Arrhenius behavior is seen at $T < 40$ K. It is inexplicable that Γ increases again at lower temperatures. A similar behavior was reported in a previous study for the $x = 0.03$ sample (shown as triangles) [17]. The finite Γ at low temperatures indicates the presence of excitation, which has been indicated in the literature; however, no convincing results have been presented. Our high-quality data allow us to conclude that the MBP is present in crystalline $Cu_{1-x}Mn_x$ below T_f as well as the structural glass of C4mimFeCl$_4$ [7]. The susceptibility $\chi'(Q)$ increases with cooling and approaches a constant value below T_f, which is expected from the temperature dependence of energy spectra in Fig. 3. The observed temperature dependence of $\chi'(Q)$ is consistent with the previous data at relatively high Q ($\geqslant 0.4$ Å^{-1}) [18,24]. The spin dynamics at small Q is discussed in Sec. IV.

Figure 5 displays the Q dependence of elastic and inelastic scattering at several temperatures for $x = 0.034$ and 0.067. The elastic scattering intensities in Figs. 5(a) and 5(c) show the magnetic contribution after subtracting the data at high temperatures. In Figs. 5(b) and 5(d), inelastic scattering intensities at around peak energies are plotted, where the peaks at $Q = 2.7$ and 3.0 Å^{-1} are due to phonons. Thus, the elastic and inelastic scattering exhibit nearly identical intensity modulation along Q at 3 K; the intensity is enhanced at $Q \sim 0$ and 1.8 Å^{-1}. The result indicates that the elastic and inelastic scatterings stem from common spin correlations in the SG state. The Q modulation is more prominent for $x = 0.067$,
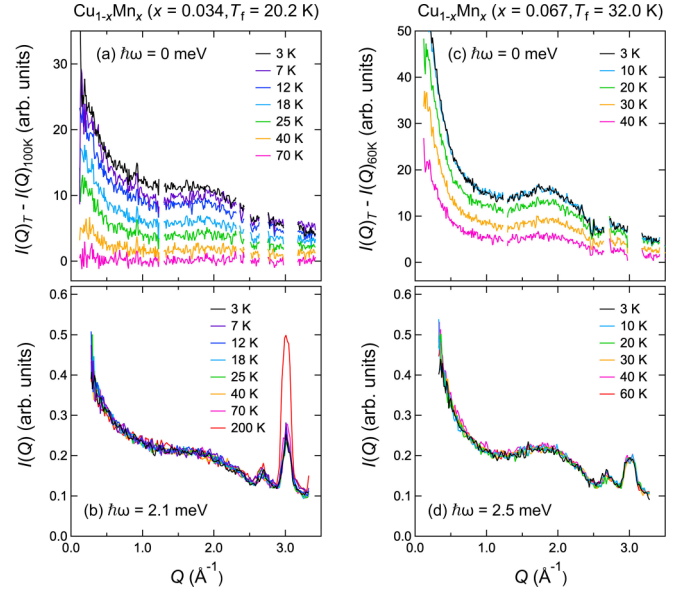
suggesting that the Mn-Mn correlation is more developed as the Mn concentration increases.

The magnetic elastic scattering gradually disappears upon heating. The temperature at which the elastic signal disappears is considerably higher than T_f because the time constant of the neutron scattering measurement is much shorter than the magnetic susceptibility measurements. The energy resolution of 0.27 meV for $E_i = 9.0$ meV corresponds to the time constant of 5 ps; fluctuation slower than the time constant is regarded as *static* in the neutron scattering measurement. This was pointed out in previous studies [18,25]. On the other hand, the Q structure of magnetic excitation does not vary with temperature in the measurement temperature range, indicating that short-range magnetic correlations are already formed at temperatures as high as 10 T_f.

The energy spectra at 3 K for all $Cu_{1-x}Mn_x$ samples are summarized in Fig. 6. Broad excitations with a high-energy tail were commonly observed in all x, although its energy scale depends on x. The higher the Mn concentration, the broader the energy spectrum. The peak energies (E_{peak}) of MBP are 1.5, 2.1, and 2.7 meV for $x = 0.017$, 0.034, and 0.067, respectively. Here, E_{peak} roughly scales with T_f. The comparison with FeAlSiO and C4mimFeCl$_4$ glasses is described later in Sec. III C.

B. FeO–Al$_2$O$_3$–SiO$_2$ glass

The temperature evolution of the INS intensity map of FeAlSiO glass is shown in Fig. 7. Broad magnetic excitation

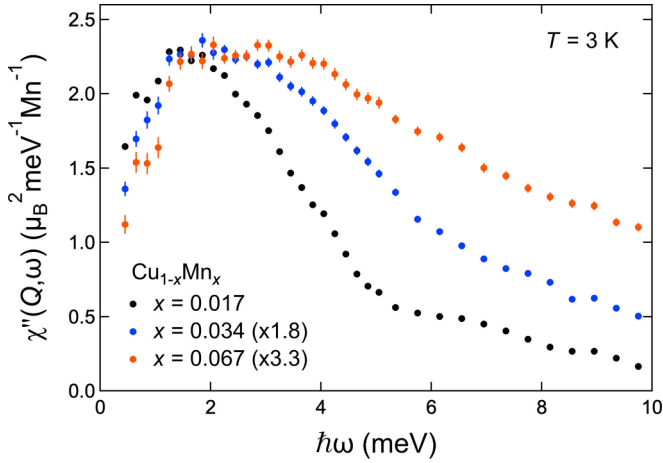FIG. 6. Comparison of $\chi''(Q, \omega)$ at $Q = [1.5, 2.1]$ Å^{-1} taken at 3 K for $Cu_{1-x}Mn_x$ ($x = 0.017$, 0.034, and 0.067). Factors are multiplied by the data of $x = 0.034$ and 0.067 for clarity.

was observed at 3 K, with strong intensity at $Q = 1.2$ Å^{-1} and $\hbar\omega = 4.5$ meV. Above T_f ($= 9.8$ K), the intensity near $\hbar\omega = 0$ increases substantially, suggesting that a magnetic relaxation process appears, and the system behaves like a liquid. Figure 8(a) shows the energy spectrum of $\chi''(Q, \omega)$ at $Q = [0.9, 1.5]$ Å^{-1} in the temperature range from 3 to 200 K. The spectrum is scaled by the Bose factor at $T < 18$ K and changes with temperature as it is raised further. The spectrum shape is
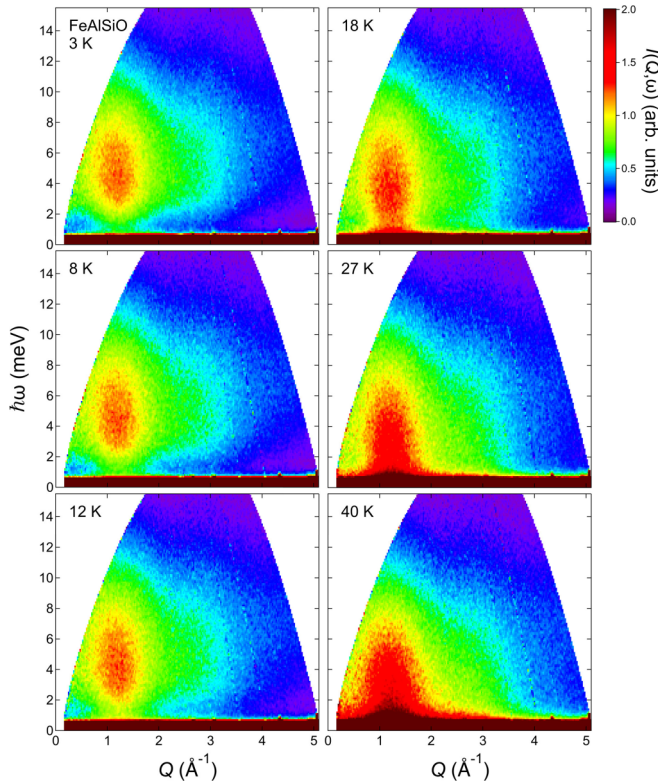

FIG. 7. Temperature dependence of the intensity map of inelastic neutron scattering (INS) of FeAlSiO glass ($T_f = 9.8$ K), measured with $E_i = 18.7$ meV.

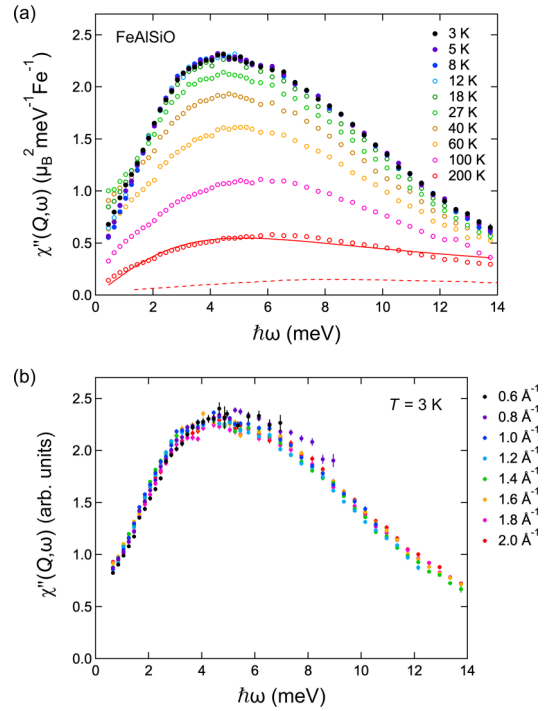FIG. 8. (a) Temperature evolution of $\chi''(Q, \omega)$ at $Q = [0.9, 1.5]$ Å^{-1} for FeAlSiO glass ($T_f = 9.8$ K). The data collected with $E_i = 5.3$, 9.0, and 18.7 meV are used. The solid curve represents a fit using the Debye relaxation model [Eq. (2)]. The dashed curve is the data at 200 K and $Q = [3.5, 4.1]$ Å^{-1}. (b) Energy spectra at several Q positions at 3 K, where scale factors are multiplied for comparison. The data collected with $E_i = 9.0$ and 18.7 meV are used.

almost independent of Q in the range of $0.6 \leqslant Q \leqslant 2.0$ Å^{-1} [Fig. 8(b)].

The solid curve in Fig. 8(a) is the result of fitting the Debye relaxation model [Eq. (2)] to the data at 200 K, with Γ of 5.1(1) meV. The unsatisfactory fit could be due to overlapping vibrational excitations, i.e., a structural boson peak in the structural glass of FeAlSiO. The data at $Q = [3.5, 4.1]$ Å^{-1} exhibit a different spectrum shape (dashed curve) and show a maximum at higher $\hbar\omega$. The vibrational contribution is remarkable at high Q, but the magnetic scattering is also present. It is difficult to separate vibrational and magnetic excitations because the energy of MPB is close to that of the structural boson peak in FeAlSiO, unlike in the case of C4mimFeCl$_4$ [7]. However, the signals at small Q and low T mostly arise from magnetic scattering. As the scattering intensity of vibrations approximately scales with Q^2, their contribution is estimated to be $<1\%$ at $Q = 1.2$ Å^{-1} below T_f.

The fits by the Debye model were performed for the data at all temperatures, although the model did not fit the data well, particularly at low temperatures. The temperature dependence of Γ showed an upturn near T_f, as seen in Fig. 4(b) for $Cu_{1-x}Mn_x$. The upturn or the finite Γ below T_f has also been reported for a related compound MnO–Al$_2$O$_3$–SiO$_2$ glass [26]. The results indicate the presence of MBP in the aluminosilicate glasses below T_f as well as $Cu_{1-x}Mn_x$ and C4mimFeCl$_4$.
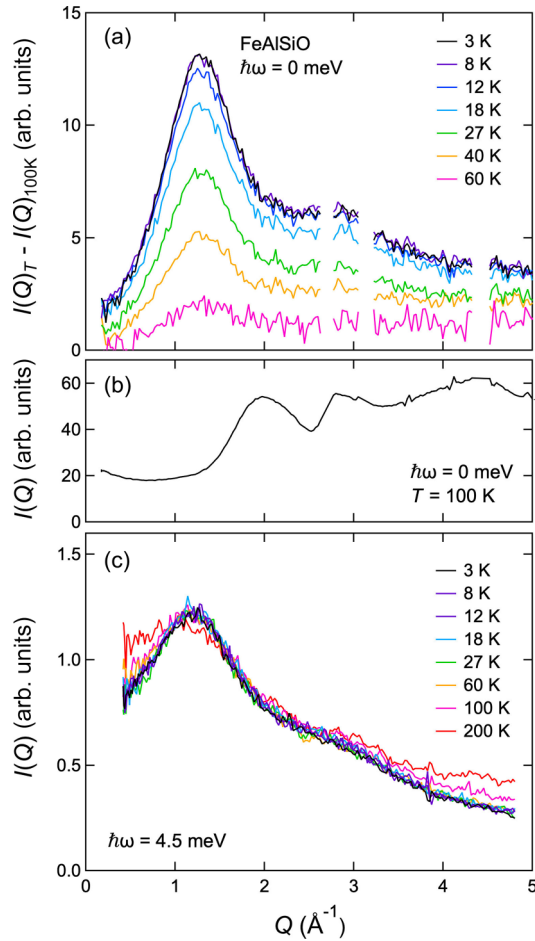
FIG. 9. (a) Temperature-subtracted elastic scattering, $I(Q)_T - I(Q)_{100K}$ obtained by integrating the data collected with $E_i = 18.7$ meV over $\hbar\omega = [-0.45, 0.45]$ meV for FeAlSiO glass. Masked regions correspond to the Bragg peaks of Al. (b) Elastic scattering at 100 K. (c) Constant-$\hbar\omega$ cuts at $\hbar\omega = [4,5]$ meV, where scale factors are multiplied for comparison. The data were collected with $E_i = 18.7$ meV.

The Q dependence of elastic and inelastic scattering is presented in Fig. 9. Magnetic elastic scattering $I(Q)_T - I(Q)_{100K}$ displayed a clear peak at $Q \sim 1.3$ Å^{-1} and a hump at twice the Q value [Fig. 9(a)]. The Q position is distinct from those of the structural (nuclear) scattering shown in Fig. 9(b), reflecting antiferromagnetic correlation. The magnetic elastic scattering weakened on heating and almost disappeared at 100 K. Inelastic signals are enhanced at the peak positions in the magnetic elastic scattering [Fig. 9(c)]. The Q structure is almost independent of temperature <100 K, but the peak broadens at 200 K ($\approx 20\,T_f$). The magnetic correlation weakens at $T \geqslant 20\,T_f$. Similar behavior was observed in C4mimFeCl$_4$ (not shown in Ref. [7]). Note that the increase in intensity at high Q and T is due to the vibrational modes.

C. Comparison among Cu$_{1-x}$Mn$_x$, FeO–Al$_2$O$_3$–SiO$_2$, and C4mimFeCl$_4$

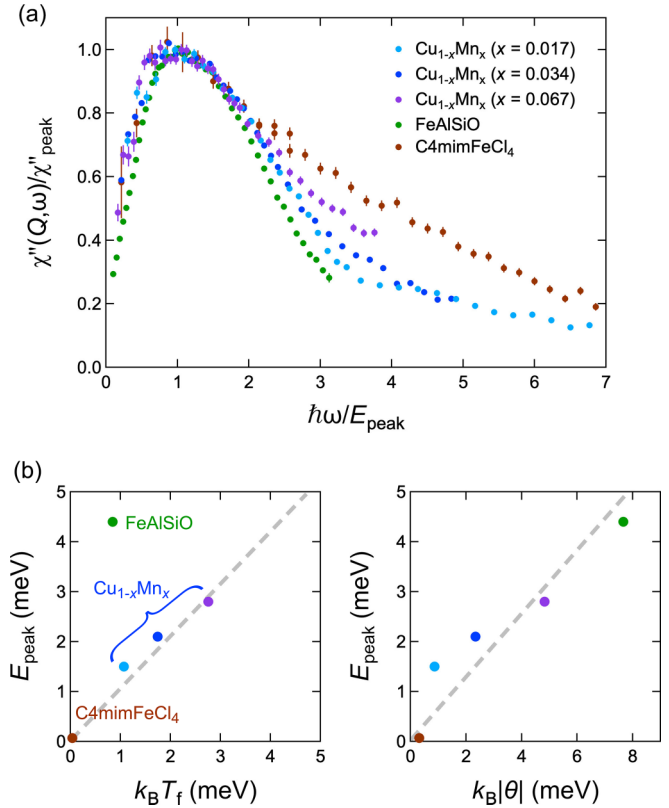Figure 10(a) shows the energy spectra of three compounds, Cu$_{1-x}$Mn$_x$ (polycrystal), FeAlSiO (amorphous), and

FIG. 10. (a) Energy spectra of Cu$_{1-x}$Mn$_x$, FeAlSiO, and C4mimFeCl$_4$ ($T_f = 0.4$ K, $\theta = -4.1$ K) [7], normalized to the peak height (χ''_{peak}) and position (E_{peak}) below T_f. (b) Peak energies against the spin-glass transition temperature ($k_B T_f$) and the magnitude of Curie-Weiss temperature ($k_B |\theta|$), where k_B is the Boltzmann constant.

C4mimFeCl$_4$ (amorphous) [7], as a function of the energy divided by E_{peak} in the SG states. The spectrum is qualitatively similar in the three compounds, with widely different T_f from 0.4 to 32 K. The shape weakly depends on the materials and could be related to their energy landscape (see Sec. IV).

The variation of E_{peak} against $k_B T_f$ and $k_B |\theta|$ are plotted in Fig. 10(b). Here, E_{peak} has an approximately linear relationship with T_f for Cu$_{1-x}$Mn$_x$ and C4mimFeCl$_4$ but not for FeAlSiO. The deviation for FeAlSiO will be discussed in Sec. IV. Meanwhile, some correlation exists between E_{peak} and $|\theta|$ for all materials, even though the data are somewhat scattered. The energy scale of magnetic excitations is not directly connected to the macroscopic parameters for systems with competing interactions. Still, a trend exists toward a higher E_{peak} for a higher T_f or $|\theta|$. Further studies on different types of SG systems are needed to gain insight into what determines the energy scale of MBP.

IV. DISCUSSION

As mentioned before, the finite Γ below T_f or the upturn in Γ indicated the presence of magnetic excitation. The behavior was previously reported in several systems including dilute magnetic alloys [17–22], metallic glass

$(Fe_{1-x}Mn_x)_{75}P_{16}B_6Al_3$ [26,27], and insulating aluminosilicate glass $Al_2Mn_5Si_4O_{16}$ [26]. For these systems, the presence of magnetic excitation has occasionally been pointed out, but no definite conclusions have been reached. The signal below T_f is very weak, which made it challenging to obtain high-quality data in the late 1970s and early 1980s when neutron scattering studies of SGs were active. The state-of-the-art spectrometer with high neutron flux enabled us to observe MBP. Furthermore, the boson peak in structural glasses became widely recognized after the 1990s. Thus, MBP might be common to classical Heisenberg SG systems, whether structurally crystalline or amorphous, metallic or insulating.

Like the structural boson peak, MBP is characterized by the broad excitation with the tail on the high-energy side. In a hierarchical model, numerous metastable valleys appear as local minima separated by finite barriers in the energy landscape [3]. Each metastable state is imposed to have a short-range correlation with a different size and spin configuration. Over-barrier hopping is allowed between the valleys at high temperatures, while the system becomes trapped in the valleys below the T_f. One can naturally imagine that excitations occur within the individual valleys. The short-range spin correlations determine their energy; excitations of small clusters appear at higher energies, whereas those of large clusters appear at lower energies. The excitation of each cluster could be described as Bose-scaled local modes, like enclosed magnons, for Heisenberg SGs. The broad spectrum is attributed to a multitude of metastable states in SGs. The observed spectrum resembles the simulation results assuming $Cu_{1-x}Mn_x$, as reported by Walker *et al.* [6]. We consider that MBP is a natural consequence of the complex energy landscape in the SG state.

The excitation characteristics of FeAlSiO are somewhat different from those of $Cu_{1-x}Mn_x$. The spectrum is narrower in energy, E_{peak}/T_f is larger (Fig. 10), and the excitations remain up to a high temperature ($\sim 2\ T_f$) in FeAlSiO. As can be seen from Table I, $|\theta|/T_f$ is ~ 10 for FeAlSiO and C4mimFeCl$_4$ and ~ 1 for $Cu_{1-x}Mn_x$. The robustness of excitation and high E_{peak}/T_f could be associated with the larger $|\theta|/T_f$. Furthermore, the frequency dependence of T_f in FeAlSiO is an order of magnitude larger than that in $Cu_{1-x}Mn_x$ [13]. Thus, T_f strongly depends on time, and the spin correlation does not grow drastically when cooling toward a critical temperature. FeAlSiO can be classified as a stronger glass than $Cu_{1-x}Mn_x$ [28]. There seems to be a tendency for systems with short-range interactions, such as magnetic insulators with $|\theta|/T_f$, to have stronger frequency dependence on T_f [29,30]. In SGs with large $|\theta|/T_f$, such as FeAlSiO and frustrated magnets, at around T_f, spin clusters are fairly well defined, and a few local minima appear in the energy landscape. The difference in the energy landscape might be related to the high E_{peak}/T_f, narrow spectrum shape, and robustness of excitation. Further investigation is needed to clarify how MBP is modified by the type of magnetic interaction and the degree of disorder or frustration.

In our investigation, we focused on the spin dynamics at $Q \geqslant 0.4$ Å^{-1}. What does MBP change in the low-Q region? In dilute magnetic alloys, such as $Cu_{1-x}Mn_x$ and $Au_{1-x}Fe_x$, with predominant ferromagnetic interaction, strong magnetic signals appear at $Q \sim 0$, and their dynamics have been in-

vestigated. At a relatively high Q ($\geqslant 0.4$ Å^{-1}), the real part of susceptibility $\chi'(Q)$ approaches a constant value below $T \simeq T_f$ [Fig. 4(c)] However, $\chi'(Q)$ exhibits a clear maximum for the data at $Q \leqslant 0.2$ Å^{-1}, which is compatible with the macroscopic alternating current susceptibility data [18,24]. The behavior at $Q \sim 0$ (large-scale spin dynamics) would differ from the high Q dynamics investigated in this paper. The early INS data suggest that the relaxation rate Γ decreases below $Q \approx 0.4$ Å^{-1} [19]. We speculate that spin waves can exist near $Q = 0$. In various structural glasses, acoustic phononlike excitations have been observed at small Q [31–34]. The excitations become obscure with increasing Q because the damping rate $\Gamma(Q)$ increases. It is discussed that the boson peak energy [$\Omega(Q)$] is closely related to the Ioffe-Regel limit [$\Omega(Q) = \pi\Gamma(Q)$ which describes a criterion of wave propagation [35,36]. However, ongoing debates on the origin of the boson peak continue.

So far, there have been no reports of observations of magnetic excitations in the low-Q region, and dedicated efforts have not been made. Meanwhile, the slow relaxation has been investigated using the neutron spin echo (NSE) technique. An investigation demonstrated that the intermediated scattering function $I(Q, t)/I(Q, 0)$, which is the Fourier transform of $I(Q, \omega)$, decays slower than the exponential function (Debye relaxation) at temperatures close to T_f [37]. Over two decades later, the nonexponential relaxation behavior was carefully examined using next-generation NSE spectrometers [38,39]. The $I(Q, t)/I(Q, 0)$ data were analyzed by a stretched exponential (Kohlrausch-Williams-Watts) function or modified forms proposed by Ogielski [40] and Weron [41]. The NSE studies show that the dynamics are independent of Q in the Q region ($Q < 0.4$ Å^{-1}). The data are not necessarily inconsistent with previous INS results [19]. The NSE data were collected in the time domain (>5 ps) corresponding to $\hbar\omega < 0.4$ meV, which is somewhat different from the dynamic range of INS measurement, although the possibility that excitations might affect the analyses cannot be ruled out. Dedicated efforts for investigating the relatively high-energy region have not been made in recent years. Detailed investigations in a wide time range using modern spectrometers are necessary to uncover the low-Q spin dynamics.

We compare the structural boson peak and MBP. The structural boson peak has the following characteristics: (i) Bose-scaled localized vibrations, (ii) broad spectrum with a high-energy tail, (iii) excess modes, (iv) peak energy of 1–5 meV, (v) intensity enhancement at structural peaks, (vi) transverse nature, and (vii) aging and pressure effects.

As mentioned above, MBP also has the characteristics of (i) and (ii). Regarding (iii), the structural boson peak is an excess of states relative to the Debye level. In other words, the localized vibrations coexist with the acoustic phonons in most glasses. The coexistence of MBP and spin waves is unclear in SGs. As for (iv), the peak energies of the structural boson peak are located at 1–5 meV for all structural glasses., while the MBP energy highly depends on materials. The E_{peak} ranges from 0.07 to 4.4 meV for the SG materials we investigated (Fig. 10). In stably existing materials, the interatomic distance is typically 1–2 Å; therefore, the strength of atomic correlations does not change by a factor of 10. However, magnetic correlations, which are determined by magnetic moments and

interactions, can vary widely from material to material, sometimes by a factor of 10 or more. It is not surprising that the excitation energy changes more significantly in magnetic systems than in structural systems.

With (v), the excitation intensity is enhanced at the diffraction peaks for both structural boson peak and MBP, although less enhancement at the first sharp diffraction peak is often reported for the structural boson peak. It indicates that the excitations are the in-phase motions, such as acoustic modes. For (vi), it has often been pointed out that the structural boson peak is intimately linked to transverse phonons but not to longitudinal ones. As typical magnons are transverse modes, MBP should have a transverse nature, at least in Heisenberg SGs.

Regarding (vii), the annealing or aging effect on the structural boson peak is often reported [42]. A decrease in the boson peak intensity and/or a high-energy shift of peak energy is found as a consequence of the relaxation of the system to more stable states. Furthermore, applying pressure shifts the boson peak energy to higher energy [8]. It would be interesting to see how MBP changes by annealing or under external magnetic fields. Experiments will be carried out in the near future.

The structural boson peak is not yet fully understood. It would be significant to study the excitation characteristics in SGs for a universal understanding of the dynamics of glassy systems. Further experimental and theoretical studies will be needed to reveal the similarities and differences between structural boson peak and MBP.

Magnetic anisotropy is a unique property of magnetic systems. Ising-like SGs without transverse components might exhibit a different spectrum shape, for instance, assembles of fine excitation peaks. It is also interesting to compare SGs with strong frustrations. Differences occur in the temperature dependence of the specific heat, effects of impurities on T_f [43], and memory effect [44,45] between archetypical and frustrated SGs. A different feature of magnetic excitation can be observed in frustrated SGs due to differences in energy landscapes.

energy with a high-energy tail. (ii) The excitation intensity is scaled by the Bose population factor below T_f. (iii) The spectrum shape does not change with momentum transfer Q, indicating localized modes. (iv) The elastic and inelastic scatterings exhibit nearly identical intensity modulations along Q. Therefore, both scatterings stem from common spin correlations in the SG state. The elastic scattering, which is static in the time scale of neutron scattering measurements, disappears at $T \sim 2\,T_f$. On the other hand, the intensity modulation of inelastic signals remains almost the same below $T \sim 10\,T_f$, suggesting robust short-range spin correlations. (v) Above T_f, the spectrum considerably changes with temperature due to the magnetic relaxation process.

The present data are consistent with the literature data taken more than 30 years ago, which were analyzed for relaxation behavior. The finite value of the relaxation rate Γ indicates the presence of magnetic excitation [17,18,24,26]. The excitation is now confirmed in our data with good statistics.

The above characteristics are like those reported for C4mimFeCl$_4$ with $T_f = 0.4$ K [7]. The observed magnetic excitation in the SG state is termed MBP by analogy with the boson peak in structural glasses. The SG materials we investigated exhibited T_f's varying considerably from 0.4 to 32 K. The energy scale of magnetic excitation is determined by the strength of magnetic correlation approximately represented by T_f or Curie-Weiss temperature. Furthermore, the broad spectrum is attributed to a multitude of metastable states in SGs. Each state is imposed to have a short-range correlation with a different size and spin configuration, and the corresponding excitation could be described as Bose-scaled local modes, like enclosed magnons.

In this paper, we demonstrate that MBP exists, regardless of whether the material is crystalline or amorphous, metallic or insulating. The Bose-scaled broad excitation peak is a general characteristic of classical systems with quenched disorders: structural and magnetic. Further studies on the aging effect and different types of materials, such as Ising-like SGs and SGs with strong frustrations, will clarify the nature of MBP with deep insights.

V. SUMMARY

We have performed INS studies on the two classical SG systems well separated from magnetically ordered phases, such as crystalline Cu$_{1-x}$Mn$_x$ ($x = 0.017$, 0.034, and 0.067) dilute alloys and iron aluminosilicate (FeAlSiO) glass, using the state-of-the-art neutron spectrometer AMATERAS. The results showed that magnetic excitations exist in their SG states. The excitations are characterized by the following aspects. (i) The INS spectrum displays a broad peak at low

ACKNOWLEDGMENTS

---

[1] K. H. Fischer and J. A. Hertz, *Spin Glasses*, Cambridge Studies in Magnetism (Cambridge University Press, Cambridge, 1991).

[2] H. Kawamura and T. Taniguchi, Chapter 1—Spin glasses, Handb. Magn. Mater. **24**, 1 (2015).

[3] J. A. Mydosh, Spin glasses: redux: an updated experimental/materials survey, Rep. Prog. Phys. **78**, 052501 (2015).

[4] K. Binder and A. P. Young, Spin glasses: Experimental facts, theoretical concepts, and open questions, Rev. Mod. Phys. **58**, 801 (1986).

[5] S. Shapiro, Chapter 5—Magnetic excitations in spin glasses, Modern Probl. Condens. Matter Sci. **22**, 219 (1988).

[6] L. R. Walker and R. E. Walstedt, Computer model of metallic spin-glasses, Phys. Rev. Lett. **38**, 514 (1977); Phys. Rev. B **22**, 3816 (1980).

[7] M. Kofu, R. Watanuki, T. Sakakibara, S. Ohira-Kawamura, K. Nakajima, M. Matsuura, T. Ueki, K. Akutsu, and O. Yamamuro, Spin glass behavior and magnetic boson peak in a structural glass of a magnetic ionic liquid, Sci. Rep. **11**, 12098 (2021).

[8] T. Nakayama, Boson peak and terahertz frequency dynamics of vitreous silica, Rep. Prog. Phys. **65**, 1195 (2002).

[9] C. Geiger, R. Newton, and O. Kleppa, Enthalpy of mixing of synthetic almandine-grossular and almandine-pyrope garnets from high-temperature solution calorimetry, Geochim. Cosmochim. Acta **51**, 1755 (1987).

[10] S. M. Dorfman, S. E. Dutton, V. Potapkin, A. I. Chumakov, J.-P. Rueff, P. Chow, Y. Xiao, R. J. Cava, T. S. Duffy, C. A. McCammon *et al.*, Electronic transitions of iron in almandine-composition glass to 91 GPa, Am. Mineral. **101**, 1659 (2016).

[11] A. F. J. Morgownik and J. A. Mydosh, High-temperature susceptibility of the CuMn spin-glass, Phys. Rev. B **24**, 5277 (1981).

[12] A. Ito, E. Torikai, H. Yamauchi, and Y. Syono, Spin glass behaviour of iron aluminosilicate glass, J. Phys. C **15**, 2759 (1982).

[13] J. P. Sanchez, J. M. Friedt, R. Horne, and A. J. V. Duyneveldt, Spin glass transition and hyperfine parameters in FeO–Al$_2$O$_3$–SiO$_2$ glasses, J. Phys. C **17**, 127 (1984).

[14] K. Nakajima, S. Ohira-Kawamura, T. Kikuchi, M. Nakamura, R. Kajimoto, Y. Inamura, N. Takahashi, K. Aizawa, K. Suzuya, K. Shibata *et al.*, Amateras: A cold-neutron disk chopper spectrometer, J. Phys. Soc. Jpn. **80**, SB028 (2011).

[15] Y. Inamura, T. Nakatani, J. Suzuki, and T. Otomo, Development status of software "Utsusemi" for chopper spectrometers at MLF, J-PARC, J. Phys. Soc. Jpn. **82**, SA031 (2013).

[16] The phonon contributions are not negligible owing to an incoherent scattering cross-section of $_{1-x}$Mn$_x$. The contribution was estimated using the relation $\chi''(\omega) \propto \omega$, that is, the density of states $\propto \omega^2$.

[17] A. P. Murani, Recent experimental studies of dynamics of spin glasses, J. Phys. Colloques **39**, C6-1517 (1978).

[18] A. Murani and J. Tholence, Spin dynamics of a binary alloy (spin glass), Solid State Commun. **22**, 25 (1977).

[19] A. P. Murani, High-temperature spin dynamics of Cu-Mn spinglasses, Phys. Rev. Lett. **41**, 1406 (1978).

[20] H. Scheuer, J.-B. Suck, A. Murani, and M. Loewenhaupt, The low temperature magnetic excitation spectrum of a CuMn spin glass alloy, J. Magn. Magn. Mater. **14**, 241 (1979).

[21] Y. Tsunoda, N. Kunitomi, and J. W. Cable, Magnetic excitation in CuMn spin glass alloy, J. Appl. Phys. **57**, 3753 (1985).

[22] J. Cable, R. Nicklow, and Y. Tsunoda, Spin dynamics of a Cu-Mn spin glass alloy, Physica B+C **136**, 318 (1986).

[23] The analyses in the previous works were performed for $I(Q, \omega)$ data, and so a simple Lorentzian function was used.

[24] A. P. Murani, Neutron scattering studies of spin-glass alloys, J. Appl. Phys. **49**, 1604 (1978).

[25] A. P. Murani and A. Heidemann, Neutron-scattering measurement of the edwards-anderson order parameter for a Cu-Mn spin-glass alloy, Phys. Rev. Lett. **41**, 1402 (1978).

[26] C. Bellouard, M. Hennion, I. Mirebeau, and B. Hennion, Insulating and metallic spin glasses: A comparative study of the dynamics by neutron scattering, J. Magn. Magn. Mater. **104-107**, 1627 (1992).

[27] I. Mirebeau and N. Martin, Revisiting neutron studies of reentrant spin glasses: The role of small-angle scattering, J. Appl. Crystallogr. **55**, 1173 (2022).

[28] J. Souletie and D. Bertrand, Glasses and spin glasses: a parallel, J. Phys. I France **1**, 1627 (1991).

[29] K. H. Fischer, Spin glasses (II), phys. stat. sol. (b) **130**, 13 (1985).

[30] J. Tholence, On the frequency dependence of the transition temperature in spin glasses, Solid State Commun. **88**, 917 (1993).

[31] P. Benassi, M. Krisch, C. Masciovecchio, V. Mazzacurati, G. Monaco, G. Ruocco, F. Sette, and R. Verbeni, Evidence of high frequency propagating modes in vitreous silica, Phys. Rev. Lett. **77**, 3835 (1996).

[32] F. Sette, M. H. Krisch, C. Masciovecchio, G. Ruocco, and G. Monaco, Dynamics of glasses and glass-forming liquids studied by inelastic x-ray scattering, Science **280**, 1550 (1998).

[33] G. Monaco, C. Masciovecchio, G. Ruocco, and F. Sette, Determination of the infinite frequency sound velocity in the glass former *o*-terphenyl, Phys. Rev. Lett. **80**, 2161 (1998).

[34] D. Fioretto, U. Buchenau, L. Comez, A. Sokolov, C. Masciovecchio, A. Mermet, G. Ruocco, F. Sette, L. Willner, B. Frick *et al.*, High-frequency dynamics of glass-forming polybutadiene, Phys. Rev. E **59**, 4470 (1999).

[35] B. Rufflé, G. Guimbretière, E. Courtens, R. Vacher, and G. Monaco, Glass-specific behavior in the damping of acousticlike vibrations, Phys. Rev. Lett. **96**, 045502 (2006).

[36] H. Shintani and H. Tanaka, Universal link between the boson peak and transverse phonons in glass, Nat. Mater. **7**, 870 (2008).

[37] F. Mezei and A. Murani, Combined three-dimensional polarization analysis and spin echo study of spin glass dynamics, J. Magn. Magn. Mater. **14**, 211 (1979).

[38] C. Pappas, F. Mezei, G. Ehlers, P. Manuel, and I. A. Campbell, Dynamic scaling in spin glasses, Phys. Rev. B **68**, 054431 (2003).

[39] R. M. Pickup, R. Cywinski, C. Pappas, B. Farago, and P. Fouquet, Generalized spin-glass relaxation, Phys. Rev. Lett. **102**, 097202 (2009).

[40] A. T. Ogielski, Dynamics of three-dimensional Ising spin glasses in thermal equilibrium, Phys. Rev. B **32**, 7384 (1985).

[41] K. Weron, A probabilistic mechanism hidden behind the universal power law for dielectric relaxation: General relaxation equation, J. Phys.: Condens. Matter **3**, 9151 (1991).

[42] S. Yannopoulos, K. Andrikopoulos, and G. Ruocco, On the analysis of the vibrational boson peak and low-energy excitations in glasses, J. Non-Cryst. Solids **352**, 4541 (2006).

[43] S. V. Syzranov and A. P. Ramirez, Eminuscent phase in frustrated magnets: a challenge to quantum spin liquids, Nat. Commun. **13**, 2993 (2022).

[44] A. Samarakoon, T. J. Sato, T. Chen, G.-W. Chern, J. Yang, I. Klich, R. Sinclair, H. Zhou, and S.-H. Lee, Aging, memory, and nonhierarchical energy landscape of spin jam, Proc. Natl. Acad. Sci. USA **113**, 11806 (2016).

[45] A. M. Samarakoon, M. Takahashi, D. Zhang, J. Yang, N. Katayama, R. Sinclair, H. D. Zhou, S. O. Diallo, G. Ehlers, D. A. Tennant *et al.*, Scaling of memories and crossover in glassy magnets, Sci. Rep. **7**, 12053 (2017).